JOURNAL OF AIRCRAFT
Vol. 32, No. 5, September–October 1995

Acoustics of a Counter-Rotating Shrouded Propfan: Prediction and Data

Klaus Heinig,* Fritz Kennepohl,† and Paul Traub‡
MTU Motoren- und Turbinen-Union München GmbH, Munich, Germany

The acoustic characteristics of a counter-rotating integrated shrouded propfan are studied both theoretically and experimentally. The calculation method comprises the main noise generation mechanisms of the propulsor as steady rotor blade loading noise, rotor/rotor and rotor/struts interaction noise, inlet flow distortion noise, and broadband noise. It accounts for flow, duct, and blade sweep effects, sound reflection from the blade rows, and propagation through inlet and nozzle. The calculation model is verified by measurements taken with a 0.4-m-diam, air turbine driven propfan model with 10 blades on each of the two rotors in the German-Dutch Wind Tunnel DNW. Deviations between calculated and measured results are attributed to mode and frequency conversion effects occurring when the sound from the rear rotor is reflected from the front rotor and when it is transmitted through the struts. A parametric study showed that the frequency and directivity characteristics of the sound field of a fan with slightly different blade numbers on both rotors are similar to those of a fan with equal rotor blade numbers. Both blade sweep and tip speed have a small influence on far-field noise, but a considerable influence on cabin noise, according to the calculation. Takeoff far-field noise can be reduced by increasing the axial distance between the rotors.

I. Introduction

WITHIN the last few years, studies in a new generation of commercial aircraft engines have concentrated on ultrahigh bypass ratio (UHB) engines. Most features of these engines rank between turbofans and open propfans. With respect to the overall economics, however, UHB engines are superior to turbofans as well as to open propfans.

One of the most promising of these concepts is the Counter Rotating Integrated Shrouded Propfan (CRISP) (Fig. 1). It is the result of an extensive configuration study,[1] which included a variety of technical and economical aspects.

The CRISP engine is characterized by a pair of counter-rotating rotors driven through a gear or from a counter-rotating turbine. Its variable-pitch blades ensure optimum operation at various mission points and provide a simple means of thrust reversal.

Compared with the open propfan, the CRISP can be installed easier under the aircraft wing. Compared with the shrouded rotor/stator fan, it gains from its high mass flow per frontal area, low blow-through drag in the engine-out (windmilling) condition and high reverse thrust.

Like all technical products, the commercial success of an aircraft engine not only depends on its economical, but also on its ecological qualities. Therefore, the noise characteristics of the CRISP have been studied both theoretically and experimentally.

II. Noise Calculation Method

The method used for the calculation of the noise emission of counter-rotating propfans includes the tone and broadband noise emission of the various blade rows and propagation effects. It incorporates both published and unpublished elements.

A. Dipole Actuator Disk Model

The calculation method is based on the assumption that the noise generated by the thin blades of modern counter-rotating propfans is predominantly dipole noise. The noise generation of the two rotors and the struts downstream of the rotors is thus simulated by means of actuator disks, which radiate their sound directly to the free field. The actuator disks consist of evenly distributed fixed, axially, and tangentially directed dipoles which, similar to Gutin's classic propeller noise theory,[2] are excited by the harmonic components of the blade air loading transformed into an absolute system. But, in contrast to Gutin's theory, the sound generation of the unsteady air loading and the influence of the flow convection is taken into account.

B. Tone and Broadband Noise Sources

The following air loadings of the actuator disks are accounted for in the calculation model:

1) The steady-state air loadings of the two rotors result from the mean flow.

2) A periodic air loading of the front rotor is generated by steady-state inlet disturbances and large-scale turbulence structures entering the intake.

3) Also, a periodic air loading of the front rotor is generated by interference between the potential flowfields of the front and rear rotors.

4) A periodic air loading of the rear rotor is caused by the viscous wake of the front rotor and by interference between the potential flowfields of the front and rear rotors.

5) A periodic air loading of the struts is caused by the wake of the rear rotor.

6) Finally, as the mechanism responsible for broadband noise, random air loadings of the rotors and struts emerge from turbulence in the boundary layer and by vortex shedding from the trailing edges of the blades and other effects.

The steady-state air loading is obtained automatically when calculating the aerodynamic parameters necessary for the acoustic calculation. However, the sound radiation associated with this air loading is not effective under takeoff and landing conditions (i.e., subsonic relative tip Mach numbers), because the sound radiation is attenuated by the cutoff effect of the fan duct.

Received Jan. 31, 1994; revision received Nov. 3, 1994; accepted for publication Feb. 21, 1995.

*Head of Unsteady Aerodynamics Department.
†Senior Acoustics Engineer.
‡Acoustics Engineer.

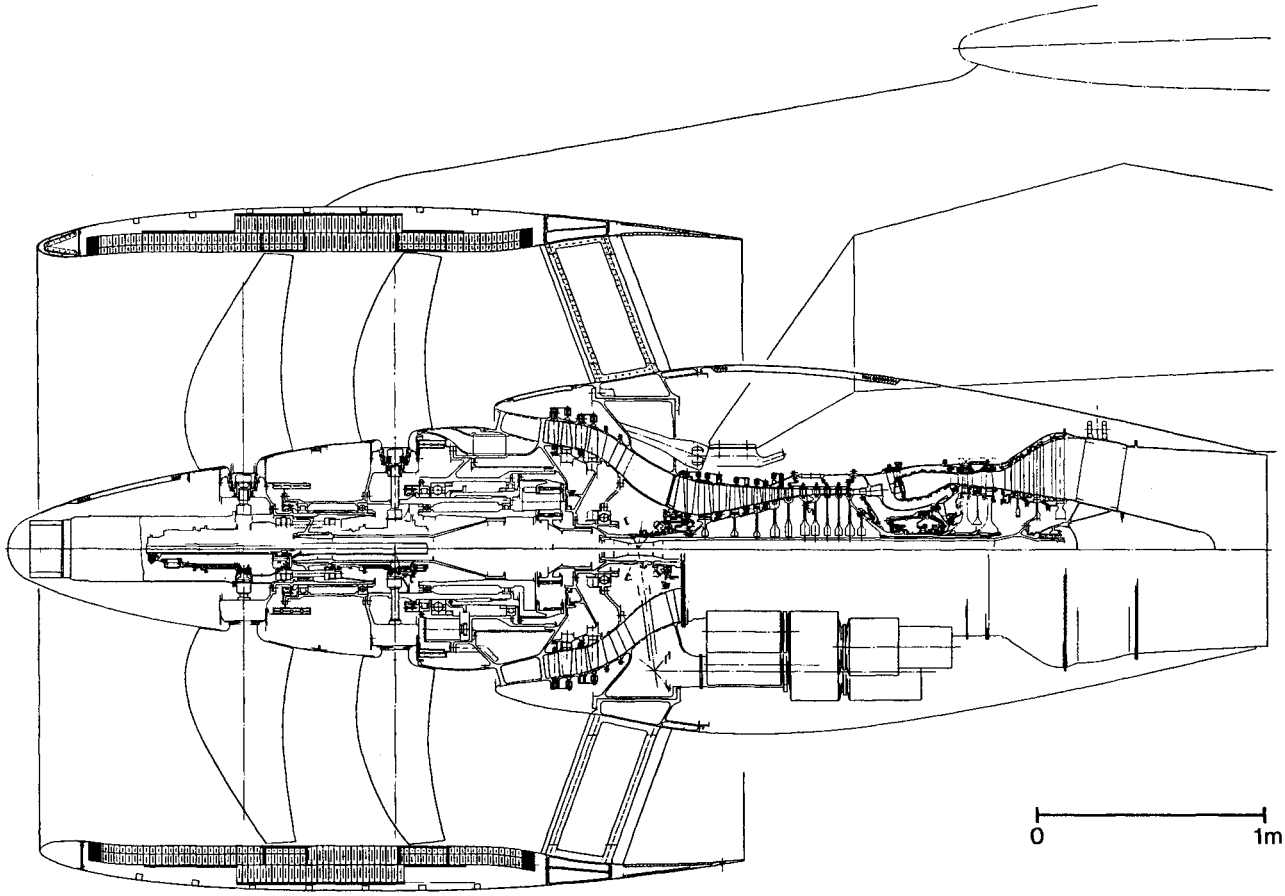

Fig. 1 CRISP engine for twin-engine 150-seat aircraft.

The periodic air loadings caused by steady-state inlet disturbances, potential flow interference, and viscous rotor wakes are calculated from the relevant velocity disturbances using the flat plate cascade theory for unsteady compressible flows developed by Smith[3] at each radial station. The velocity disturbances associated with potential flow interference can be determined from the circulation flowfield of the other rotor. The velocity distribution of the viscous rotor wakes can be determined from their geometry and flow parameters using Silverstein's correlation.[4]

The periodic air loading resulting from large-scale turbulence structures can be calculated by the correlation according to Hanson,[5] which supplies the amplitudes of the air loading harmonics in relation to the steady-state air loading. These are effective amplitudes that allow for the correlation length of the air loading.

The random air loading is described by an empirical equation for the power spectral density. The equation includes the steady-state air loading, the blade surface area, and a Strouhal number formed with the blade chord length and the cascade entry velocity.

C. Duct Effects

The sound fields or modes generated by the individual air-loading harmonics have the same structure as the air-loading harmonics in the azimuthal direction. This structure can be described by a mode number. This number, the sound frequency, and the axial flow velocity can be used to determine if the individual sound modes in the duct housing the cascade can propagate either with or without attenuation. That is to say, the sound modes can be split into cutoff and cuton modes. The cutoff effect of the duct can be taken into account by ignoring the contribution of the cutoff modes to the sound emission of the propfan. This effect represents the main influence of a cylindrical flow duct on the sound propagation. As the investigations by Wright,[6] Rice,[7] and Candel[8] have shown, a cylindrical flow duct is only of secondary significance with regard to the sound radiation of the cuton modes.

D. Sound Propagation Through Cascades

The noise calculation method also makes allowance for the losses occurring when the sound modes propagate through the rotors and struts, particularly as a result of reflection. These sound propagation losses are calculated using a procedure developed by Koch,[9] which is based on a plate cascade model and supplies a sound transmission coefficient. The input parameters are the cascade geometry, flow velocity in the cascade duct, frequency, and angle of incidence of the sound mode.

E. Sound Propagation Through Inlet and Nozzle

The sound radiated by the inlet and nozzle is corrected with regard to directional and level variations occurring in the inlet and nozzle flow, using a ray theory.

As the velocity gradients in the flow are relatively small, the deflection that occurs as the sound propagates through the inlet flow must be attributable above all to differences in the convection of the sound waves inside and outside the inlet. Therefore, when calculating the deflection it is assumed that the vector of the wave-normal retains its direction within the inlet flow and that the direction of the sound ray (intensity vector) varies only as a result of differences in the axial velocity inside and outside the inlet. The change in the sound level is associated with the fact that the deflected ray transports the same acoustic power as is transported by the ray leaving the inlet.

In determining the acoustic refraction in the flow through the nozzle, for the sake of simplification it is assumed that the nozzle flow is separated from the surrounding fluid by a thin cylindrical shear layer, in which the flow velocity, the

fluid density and velocity of sound change. This approach allows the refraction and reflection at the shear layer to be determined in accordance with the ray theory using the relations given by Morse and Ingard.[10]

III. Model Tests

A. Model

In order to verify the CRISP noise predictions, noise measurements were taken with a 0.4-m-diam model. This model was originally designed to evaluate and demonstrate the aerodynamic performance potential of the propulsor and to establish the technological basis for a final configuration. Whereas a large-scale CRISP engine will have composite blades of high AR (see Fig. 1), the model has titanium blades, whose chord lengths have to be wider due to mechanical reasons. Because the relative distances between the model rotors and between the rear rotor and the struts are extremely small, its noise emission is expected to be higher and its noise source breakdown to be different from that of a large-scale fan; the measurements, however, can be used to verify the calculation method.

The model has 10 + 10 rotor blades and 7 struts. It can be modified, by exchanging some parts, in order to utilize 12 blades at the rear rotor and an increased axial spacing between front and rear rotor. The rotors are driven by an air turbine through a gear and rotate with the same speed in opposite directions.

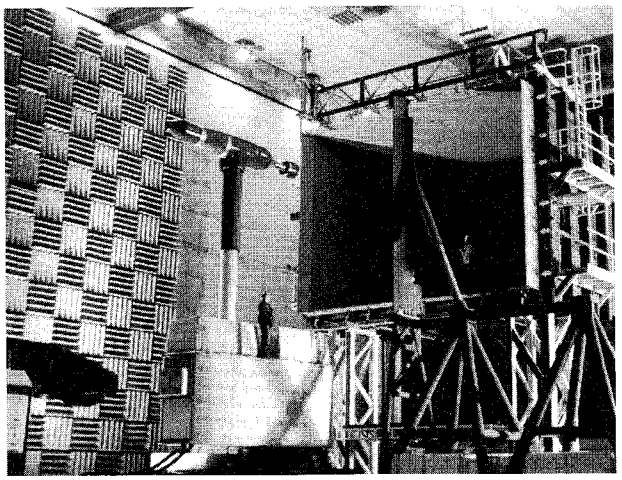

Fig. 2 CRISP model tests in the DNW, November 1991.

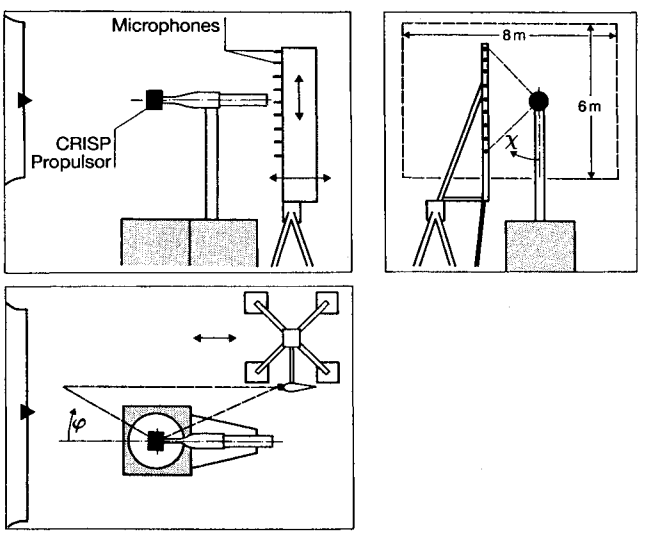

Fig. 3 Arrangement of model and microphone rake in the DNW.

B. Test Setup and Instrumentation

The configuration with 10 + 10 blades and short axial spacing between the rotors was tested in November 1991 in the German-Dutch Wind Tunnel DNW. The arrangement of the CRISP model in the 6 × 8 m open jet "acoustic" configuration of the wind tunnel is shown in Fig. 2. Inflow far-field measurements were taken with a microphone rake traversing parallel to the model axis. Figure 3 includes the range of polar and azimuthal angles covered by the microphone rake. Angles of attack could be tested by rotating the model support about a vertical axis, with the shroud fixed in a 90 deg turned position, so that the microphone rake covers the angular range below the aircraft in a real flyover situation. More details about the far-field noise measurements are given in Ref. 11.

In addition to the far-field noise levels, the mode distribution within the shroud was measured at some operating conditions, with the microphones traversing circumferentially in the shroud exit plane. The instrumentation, data acquisition, and analysis are described in detail in Ref. 12.

C. Test Program and Results

The far-field noise test program included variations of 1) fan pressure ratio $[(\mathrm{FPR} - 1)/(\mathrm{FPR}_{\mathrm{Design}} - 1) = 0.2, 0.4, 0.6, 0.8, 1.0]$; 2) blade stagger angle, at various FPRs, to allow an acoustic optimization of the stagger angle/rotational speed combination with respect to noise; 3) tunnel Mach number (up to 0.23); 4) angle of attack (up to 20 deg).

Out of the extensive data only some main results shall be given here; some additional information is presented in Ref. 11:

1) At high fan pressure ratios, the noise of the model is dominated by interaction tone noise, with the highest tone levels occurring at the third harmonic of the blade passing frequency (3 BPF).

2) At lower FPRs, the broadband noise dominates.

3) The maximum perceived noise level, tone-corrected (PNLT) of a scaled 2.5-m-diam fan occurs at a polar angle of 120–130 deg to the inlet axis.

4) The influence of stagger angle or rotational speed at constant FPR is small within the tested (already preoptimized) range.

5) The shroud provides for unseparated flow up to an angle of attack of 24 deg at Mach 0.175. Separated flow at the shroud inlet lip would lead to excessive noise levels due to the highly distorted rotor inlet flow.

6) The azimuthal directivity pattern, measured by moving the microphone vertically, is periodic with the angle between two encounter positions of the rotors (360 deg/20), and/or with the angle between two struts (360 deg/7).

7) Variations of the sideline distance of the microphone rake proved that the far-field condition was sufficiently fulfilled at the standard distance of five diameters, to yield reliable PNLT distributions along the sideline.

The measurements taken in the shroud exit plane revealed the following:

1) The modes generated by the aerodynamic interaction of the blade rows exhibit the highest amplitudes.

2) At the BPF the interaction between the rear rotor and the struts is the dominating noise mechanism.

3) At higher tone harmonics, contributing more efficient to the PNLT, the rotor/rotor interaction dominates clearly.

4) The modes generated by rotor/rotor interaction are partially converted into other modes when they propagate through the struts.

IV. Comparison of Calculated and Measured Noise Characteristics

A. Azimuthal Directivity Pattern

If the measurements taken at various azimuthal angles along sidelines parallel to the model axis are converted to the same

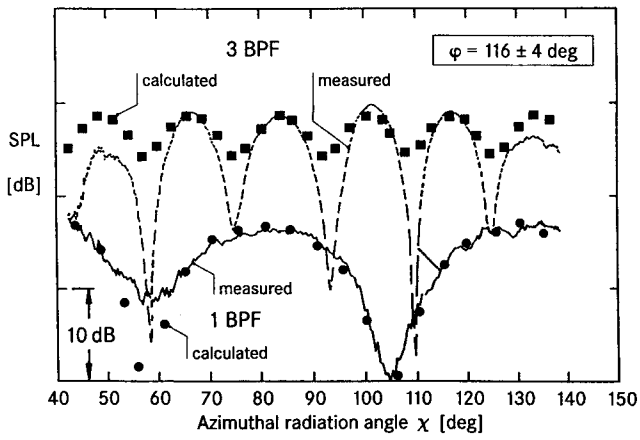

Fig. 4 Comparison of calculated and measured azimuthal directivity patterns.

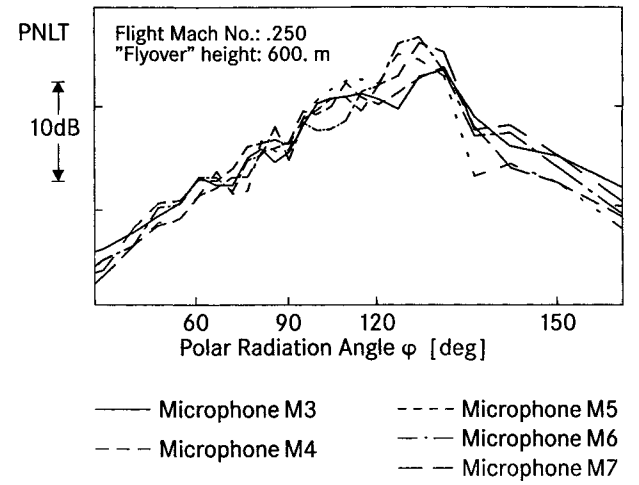

Fig. 5 Comparison of polar PNLT directivities measured at various azimuthal angles.

sideline distance, differences are visible, as expected. To obtain more detailed information about the azimuthal distribution, additional traverses were carried out by moving the microphone rake up and down at fixed axial positions. These measurements revealed generally complicated patterns of the tone harmonic levels.

As an example, Fig. 4 shows measured azimuthal directivity patterns of the BPF and the 3 BPF tones at a polar angle of 116 deg. The relative fan pressure ratio is (FPR − 1)/(FPR$_{Design}$ − 1) = 0.8, representing a full thrust takeoff operating condition. In this case, the levels of both tones exhibit regular patterns. They are periodic with the number of struts (7) in the case of the BPF tone and with the number of rotor blade encounter positions (20) in the case of the 3 BPF tone. This is not surprising, because, as will be shown later, the BPF tone is mainly generated at the struts, due to interaction with the rear rotor wake, whereas the 3 BPF tone is mainly generated at the rear rotor, due to interaction with the front rotor wake. Figure 4 shows that these azimuthal patterns are recovered with the calculation method described earlier. It is interesting to note that rotor/rotor interaction tones at even harmonic numbers (2, 4, 6 BPF, etc.) do not vary in amplitude along the azimuthal angle, according to the calculation.

The pronounced azimuthal directivity patterns at some harmonics could suggest a possible optimization of the noise from a CRISP engine received on the ground by a rotation of the engine about its axis. However, the azimuthal patterns of the tones vary with polar angle, i.e., the level minima along the azimuthal angle do not occur at the same position at different polar angles. In a real flyover situation, therefore, differences tend to cancel out, because a wide range of polar angles contributes to the effective perceived noise level (EPNL) metric.

Figure 5 gives an impression of the differences between the noise measured at various azimuthal angles in terms of PNLT (of a scaled 2.5-m-diam fan at a sideline distance of 600 m) vs polar angle. It can be seen that these differences are small. A considerable reduction of the CRISP noise in terms of EPNL, therefore, is not possible by a rotation about the engine axis.

B. Frequency Spectrum

For further analysis the levels measured at the various azimuthal angles were averaged energetically to get the polar distribution of the spectrum. From this, the sound power spectrum was calculated. Figure 6 shows the measured one-third-octave band sound power spectrum for a takeoff operating condition. Also included in the figure are calculated noise spectra for the front rotor, the rear rotor, the struts, and the sum of all three rows. The aerodynamic input data, including the aerodynamic loss factors of the rotors along the radius, were evaluated with a streamline curvature method, using the measured radial distribution of total pressure along the leading edge of the struts as an input. The noise calculation includes tones up to the 23rd tone harmonic, corresponding to measured data up to the upper limit of the 40-kHz one-third-octave band.

It can be seen that with the method described, the measured tone noise spectrum is recovered with satisfactory accuracy at the BPF and at high frequencies, where a high number of tones is involved in each frequency band. In the midfrequency region, however, considerable differences occur. The rotor/rotor interaction dominates the overall propulsor noise by far. Only the BPF tone, which does not contribute considerably

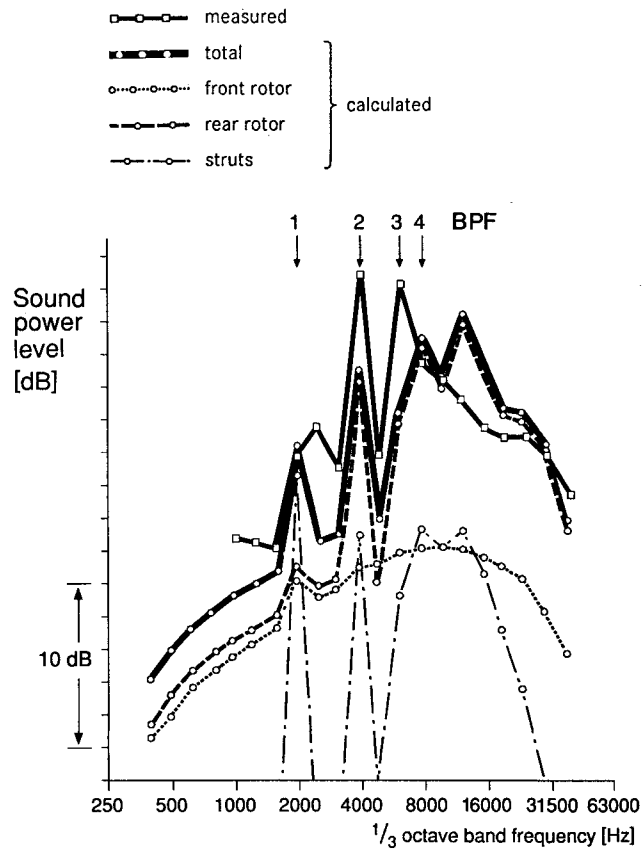

Fig. 6 Comparison of calculated and measured sound power spectra.

to the far-field PNLT, is generated mainly by the interaction between the rear rotor and the struts.

The broadband noise spectrum could not be recovered by the calculation method, using the empirical law for the random air loading gained from another fan. Therefore, the random air-loading curve was adjusted in peak level and frequency to fit the measured broadband noise spectrum of the CRISP. This spectrum was evaluated from the measured narrow-band spectrum by substituting the level of each tone at a multiple of the rotor shaft frequency by the average between the levels of the two adjacent narrow bands. It was found that the measured broadband noise spectrum is recovered reasonably well, if the peak frequency of the spectrum of the random air-loading is evaluated with a Strouhal number (based on the chord length) considerably higher than one. This leads to the conclusion, that the random air loading is at least partially caused by mechanisms whose characteristic lengths are smaller than the chord length, e.g., the boundary-layer displacement thickness.

At the operating condition of Fig. 6, the broadband noise is seen to play a minor role. At lower fan pressure ratios, however, its contribution to the overall noise becomes more important. Furthermore, the axial distance between the rotors is extremely small at the model, leading to much higher interaction tone noise levels than with the projected full-scale engine (Fig. 1). The broadband noise, therefore, will be more important for the full-scale engine.

In addition to the tone noise at multiples of the BPF and the broadband noise, a considerable amount of tone noise at multiples of the rotor shaft frequency was measured. This is visible, e.g., in Fig. 6 between the BPF and the 2 BPF tones, exceeding the level at the BPF. This noise source is probably caused by slight differences between the rotor blades and should not be evident for a full-scale engine.

C. Polar Directivity Pattern

The measured polar directivity patterns of the tone harmonics, most of which peak in the aft quadrant at a polar angle of around 120 deg, cannot be recovered by the calculation model at higher frequencies. The reason for this is the fact that modes of the hf sound emitted by the rear rotor are converted partially into other modes when they are reflected by the front rotor. Moreover, these modes are shifted to other frequencies. The directivity of these converted modes, however, cannot be determined with the current calculation model.

D. Mode Distributions

Due to the various tone-generating mechanisms, the following modes, characterized by their frequencies and mode orders m (m is positive if the mode rotates in the same direction as the rear rotor), are generated by a counter-rotating fan:

1) Interaction between inlet distortions and front rotor:

$$\omega = j_1 B_1 \Omega_1$$

$$m = -j_1 B_1 \pm L$$

2) Interaction between inlet distortions and rear rotor:

$$\omega = j_2 B_2 \Omega_2$$

$$m = j_2 B_2 \pm L$$

3) Interaction between front and rear rotor:

$$\omega = K_1 B_1 \Omega_1 + K_2 B_2 \Omega_2, \qquad \omega > 0$$

$$m = K_1 B_1 - K_2 B_2, \quad K_1, K_2 \text{ positive or negative integers}$$

Table 1 Modes generated by the CRISP model

Mechanism	j	m
1, 2	1	$-6, -5, \ldots, 7, 8$
	2	$-13, -12, \ldots, 16, 17$
3	1	None
	2	0
	3	$-10, 10$
	4	$-20, 0, 20$
4	1	$-4, 3$
	2	$-8, -1, 6, 13$
	3	$-19, -12, -5, 2, 9, 16, 23$
5	1	$-3, 4$
	2	$-13, -6, 1, 8, 15$
	3	$-16, -9, -2, 5, 12, 19, 26$

4) Interaction between rear rotor and struts:

$$\omega = j_2 B_2 \Omega_2$$

$$m = j_2 B_2 \pm KV, \qquad K \text{ integer}$$

5) Interaction between front rotor and struts:

$$\omega = j_1 B_1 \Omega_1$$

$$m = -j_1 B_1 \pm KV, \qquad K \text{ integer}$$

Here, B_1, B_2, and V are the blade numbers of the front rotor, rear rotor, and the struts, respectively; Ω_1 and Ω_2 are the rotational speeds of the front and rear rotor; L is the circumferential order of the inlet distortion (caused, e.g., by an angle of attack); and j_1 and j_2 are the tone harmonic orders of the front and rear rotor, respectively. For the case of the CRISP model ($B_1 = B_2 = 10$, $V = 7$, and $\Omega_1 = \Omega_2$) at a typical takeoff operating condition, taking into account the cutoff criterion, Table 1 shows the modes generated by the previously mentioned mechanisms.

Whereas the modes due to inlet distortions (mechanisms 1, 2) are low in amplitude due to the excellent tunnel flow quality and an inlet causing little distortions, the rotor/rotor and rotor/struts interaction modes carry high energies, as seen in Fig. 6. In fact, these modes were found to have high levels in the shroud exit plane of the model. Figure 7 presents the measured mode distribution at the first four BPF harmonics at takeoff. These measurements confirm the fact already found by calculation (see Fig. 6), that the rotor/strut interaction causes the highest level at the BPF, but at the more important higher harmonics the rotor/rotor interaction dominates.

In addition to the modes listed above, some others exhibit unexpectedly high amplitudes. As shown in Ref. 12, these modes can be explained by a conversion of rotor/rotor interaction modes when they propagate through the struts. The mode orders of the converted modes can be shown to fulfill the relation

$$m_c = m \pm KV, \qquad K \text{ integer}$$

where m is the primary mode incident on the struts, generated by the rear rotor.

V. Parametric Study

With the method described earlier, the noise of a 2.5-m-diam full-scale engine was calculated. A parametric study was included as a basis for a further acoustic optimization of the CRISP.

A. Blade Numbers

As a first step, the influence of the rotor blade numbers on takeoff and cruise noise was evaluated on the basis of equal blade numbers of front and rear rotor. It was assumed that

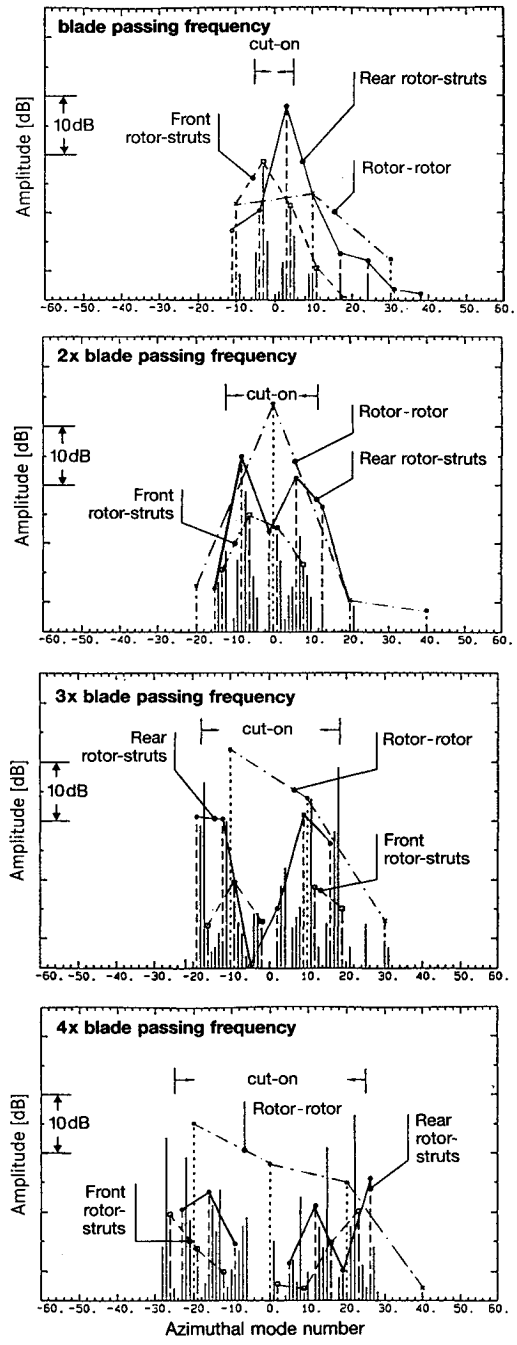

Fig. 7 Mode distribution measured in the shroud exit plane.

the steady-state airloading of the blades varies inversely proportional to the blade number. Whereas differences in takeoff EPNL were found to be small, the blade number has a pronounced effect on the cabin noise. This is due to the cabin wall sound transmission characteristic, which was calculated here with a simple one-dimensional double-wall model (see Fig. 8), together with the change of BPF with the blade number. For example, with 10 + 10 blades instead of 12 + 12, the cabin noise in the rotor plane would increase by as much as 4.5 dBA. Therefore, the rotor blade number has to be as high as possible from the acoustic point of view. Because of the low hub-to-tip radius ratio of the CRISP concept, however, the blade numbers cannot be increased considerably above 12.

If the blade numbers or rotational speeds of the front and the rear rotors are different from each other, the frequency spectrum exhibits additional tones. Of the tones produced by rotor/rotor interaction, the frequencies being given earlier,

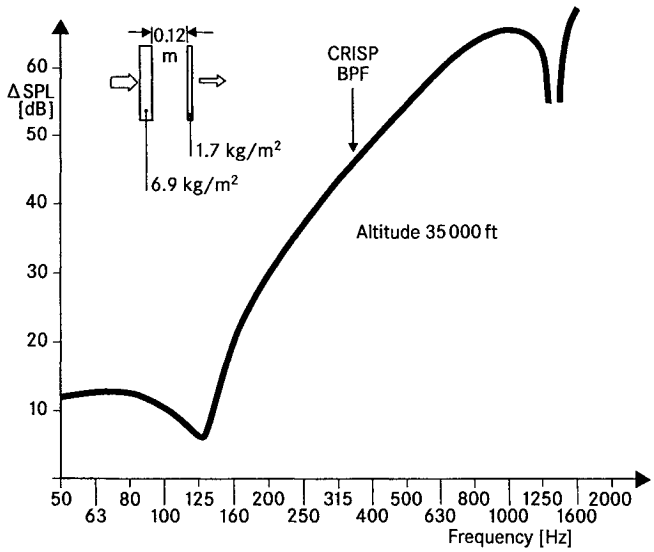

Fig. 8 Frequency characteristic of a typical cabin wall.

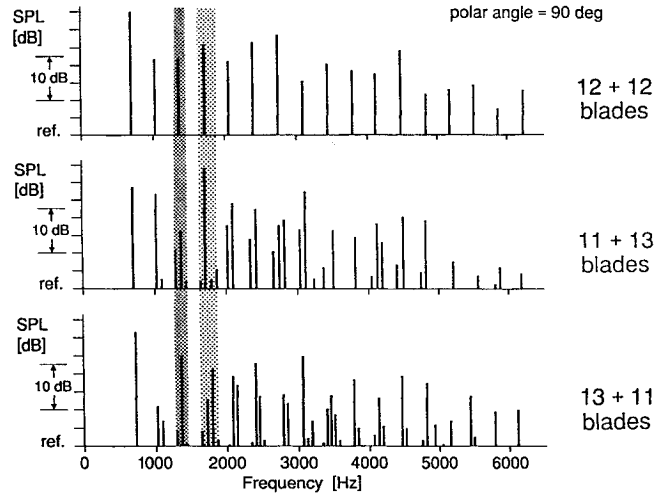

Fig. 9 Interaction tone noise spectra of CRISP with equal and different blade numbers.

only those at the following frequencies have considerable amplitudes, due to cutoff reasons:

$$\begin{array}{llll} \omega_1 & \omega_2 & & \\ 2\omega_1 & \omega_1 + \omega_2 & 2\omega_2 & \\ 3\omega_1 & 2\omega_1 + \omega_2 & \omega_1 + 2\omega_2 & 3\omega_2 \\ \text{etc.} & & & \end{array}$$

Here, ω_1 and ω_2 are the blade passing frequencies of the front and rear rotor, respectively ($\omega_{1,2} = B_{1,2} \times \Omega_{1,2}$). It can be seen that each tone of a fan with equal blade numbers on front and rear rotors is split up into a cluster of tones in the case of (slightly) different blade numbers. The frequencies arranged in one line belong to a cluster. The first and the last frequency in each line represent rotor alone tones, all others represent interaction tones.

As an example, Fig. 9 shows calculated noise spectra of the rear CRISP rotor due to aerodynamic interaction with the front rotor, for the blade number combinations 12 + 12, 11 + 13, and 13 + 11, the rotational speeds of both rotors being equal in all three cases. Figure 10 presents the directivity pattern of these tones at the second and third harmonic. It is found that if the contributions of each cluster are summed up energetically, the three configurations 12 + 12, 11 + 13, and 13 + 11 are similar in level and polar angle distribution. This

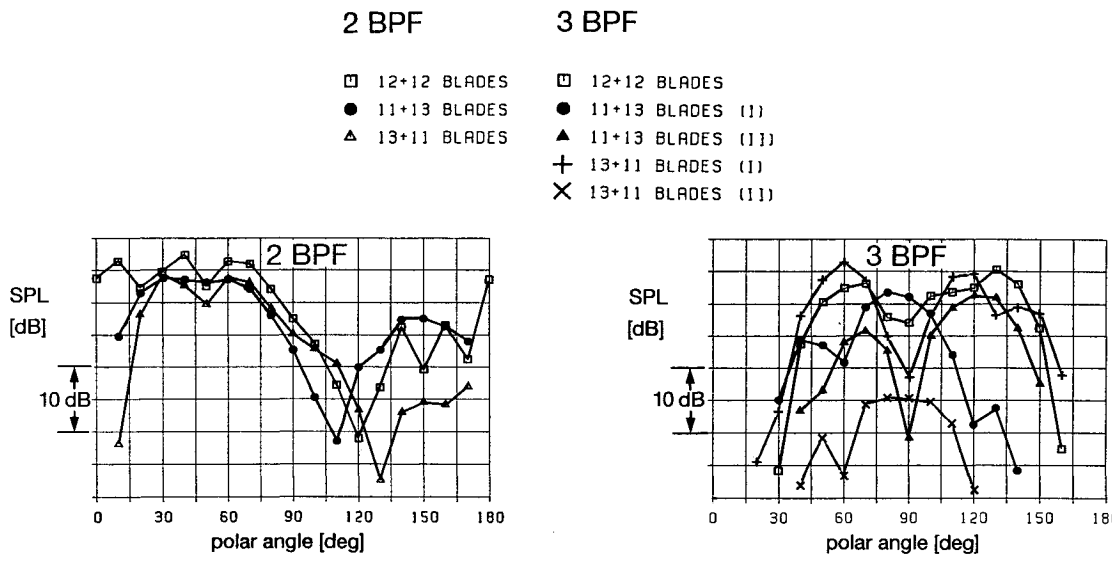

Fig. 10 Interaction tone noise directivities of CRISP with equal and different blade numbers.

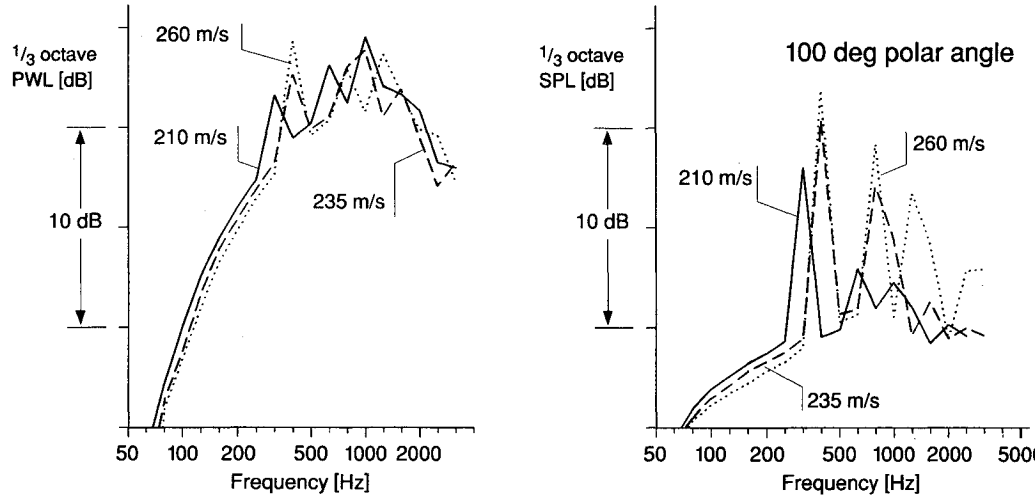

Fig. 11 Influence of tip speed on takeoff and cruise noise spectra.

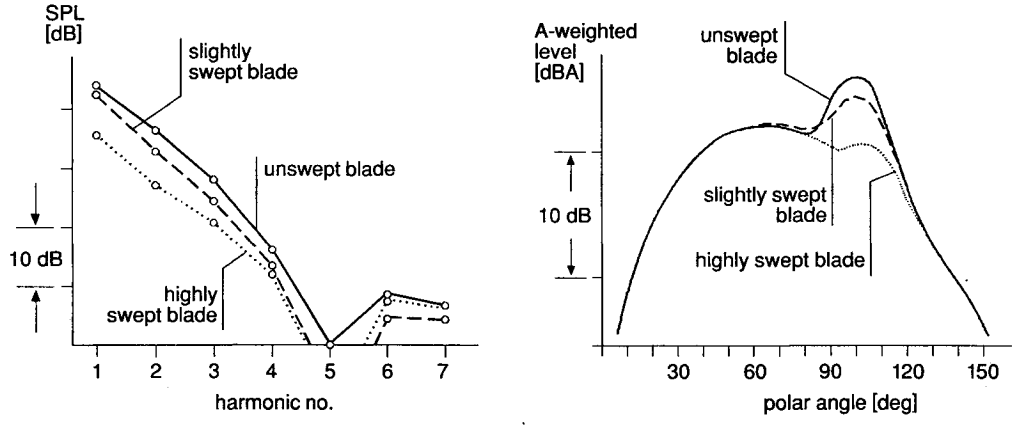

Fig. 12 Influence of blade sweep on cabin noise at cruise.

is not surprising because, e.g., the plane wave $m = 0$, occurring with the 12 + 12 configuration at the second harmonic, is shifted towards $m = \pm 2$ in the case of 11 + 13 or 13 + 11, i.e., a mode whose wave-normal forms a small angle to the propeller axis. (Mode orders m up to about 15 are cuton at the second harmonic.) Also, the one-third-octave band sound power spectra of the three configurations look very similar and the calculated EPNLs of an aircraft equipped with these configurations are only slightly different. A small potential for tuning the blade numbers to minimize airport noise, however, is seen due to the differences in subjective noise levels. For example, the tone correction of the PNLT calculation can be reduced by distributing the tones more evenly over the one-third-octave frequency bands.

B. Tip Speed

Figure 11 shows the influence of the tip speed on the CRISP noise spectra at takeoff and cruise. Fan pressure ratio and mass flow are kept constant. At both operating conditions, the amplitude of the BPF tone increases with tip speed. However, the influence on takeoff (sideline) EPNL was found to be small. The cabin noise at cruise in terms of dBA increases with tip speed, but with a much smaller gradient than the free-field level at cruise, because of the frequency dependence of the cabin wall transmission loss.

C. Blade Sweep

Calculations with various blade shapes were done to evaluate the influence of blade sweep on noise. At takeoff operating condition only a small effect was found. The noise reduction at cruise is shown in Fig. 12. The cabin noise is caused mainly by the steady-state air loading. The contributions of the various radial portions of this air loading to the far-field sound pressure exhibit phase differences in the case of a swept blade, leading to a smaller amplitude of the sum sound pressure from all radial portions. Figure 12 shows that this effect works for the BPF as well as for higher harmonics, and that the noise reduction increases with sweep angle. The curve marked "slightly swept" belongs to the blade shape shown in Fig. 1. High sweep angles are difficult to realize with variable pitch blades and a shroud, as the tip clearances must be kept small.

Also, Fig. 12 shows that with the CRISP the noise floor resulting from the outer fuselage wall boundary layer is exceeded only by a small amount in terms of dBA.

D. Axial Distance Between Rotors

Finally, the influence of the axial rotor-to-rotor distance on noise was evaluated. Because the rotor/rotor interaction is the dominating tone noise mechanism at takeoff and landing conditions, this parameter affects primarily the airport noise levels. As expected, the calculations showed that the takeoff (sideline) EPNL can effectively be reduced by increasing the relative spacing between the rotors.

VI. Concluding Remarks

The various noise sources of the CRISP as steady-state rotor blade loading noise, rotor/rotor and rotor/stator interaction noise, inlet distortion noise, and broadband noise were calculated with a dipole actuator disk method. The sound propagation through blade rows, inlet, and nozzle was taken into account.

The results were compared to measurements with a 0.4-m-diam counter-rotating shrouded fan model with 10 blades on each rotor. The comparison showed that the model predicts the main noise characteristics fairly well. Deviations in the spectrum and the polar directivity characteristic are attributed to mode and frequency conversion of the rotor/rotor interaction noise as it is reflected from the front rotor. Furthermore, mode measurements showed that rotor/rotor interaction modes are converted into other modes as they propagate through the struts.

A parametric study gave the following results: The frequency and directivity characteristics of a fan with different blade numbers on both rotors are similar to those of a fan with equal blade numbers. Blade sweep and design tip speed have only a small influence on takeoff far-field noise, but a considerable influence on cabin noise at cruise. The takeoff noise can effectively be reduced by increasing the axial distance between both rotors.

Airport noise predictions for a 150-seat aircraft with well-designed CRISP engines indicate that the ICAO Annex 16 noise limits can be met with a comfortable margin.

Acknowledgments

The CRISP technology program of MTU Motoren und Turbinen Union was funded by the German Ministry of Research and Technology. The assistance of the Deutsche Forschungsanstalt für Luft- und Raumfahrt DLR at Braunschweig, Berlin, and Göttingen, as well as of the German-Dutch Wind Tunnel DNW, is appreciated.

References

[1]Geidel, H. A., and Eckardt, D., "Gearless CRISP—The Logical Step to Economic Engines for High Thrust," 9th International Symposium on Air Breathing Engines, ISABE 89-7116, Athens, Sept. 1989.

[2]Gutin, L., "On the Sound Field of a Rotating Propeller," NACA TM 1195, Oct. 1948.

[3]Smith, S. N., "Discrete Frequency Sound Generation in Axial Flow Turbomachines," Univ. Engineering Dept., Reports and Memoranda 3709, Cambridge, England, UK, 1972.

[4]Silverstein, A., Katzoff, F., and Bullivant, W. K., "Downwash and Wake Behind Plain and Flapped Airfoils," NACA Rept. 651, 1939.

[5]Hanson, B. H., "Study of Noise Sources in a Subsonic Fan Using Measured Blade Pressures and Acoustic Theory," NASA-CR-1574, Aug. 1975.

[6]Wright, S. E., "Waveguides and Rotating Sources," *Journal of Sound and Vibration*, Vol. 25, No. 1, 1972, pp. 163–178.

[7]Rice, E. J., Heidmann, M. F., and Sofrin, T., "Modal Propagation Angles in a Cylindrical Duct with Flow and Their Relation to Sound Radiation," AIAA Paper 79-0183, Jan. 1979.

[8]Candel, S. M., "Acoustic Radiation from the End of a Two-Dimensional Duct, Effects of Uniform Flow and Duct Lining," *Journal of Sound and Vibration*, Vol. 28, No. 1, 1973, pp. 1–13.

[9]Koch, W., "On the Transmission of Sound Waves Through a Blade Row," *Journal of Sound and Vibration*, Vol. 18, No. 1, 1971, pp. 111–128.

[10]Morse, P. M., and Ingard, K. U., *Theoretical Acoustics*, McGraw-Hill, New York, 1968.

[11]Dobrzynski, W., Gehlhar, B., and Böttcher, J., "Aeroacoustic Wind Tunnel Testing of a Counter Rotating Shrouded Propfan Model," DGLR/AIAA Aeroacoustics Conf., Paper 92-02-436, Aachen, Germany, May 1992.

[12]Holste, F., and Neise, W., "Experimental Determination of the Main Noise Sources in a Propfan Model by Analysis of the Acoustic Spinning Modes in the Exit Plane," DGLR/AIAA Aeroacoustics Conf., Paper 92-02-438, Aachen, Germany, May 1992.